

Supporting Information

Porous MOFs with Geometric Mismatch between Trimers and Octatopic Pyrene-Based Ligands for Low-Temperature Methane Storage

Kun Wang, †^{a, b} Honghao Cao, †^{a, b} Yuanlong Zhong, ^{a, b} Zhenning Yang, ^{a, b} Hancheng Shi, ^c Zhangyi Xiong, ^{a, b} Yuqiao Mu, ^{a, b} and Zhijie Chen ^{a, b*}

^a Stoddart Institute of Molecular Science, Department of Chemistry, Zhejiang Key Laboratory of Excited-State Energy Conversion and Energy Storage, State Key Laboratory of Silicon and Advanced Semiconductor Materials, Zhejiang University, Hangzhou 310058, P. R. China

^b Zhejiang-Israel Joint Laboratory of Self-Assembling Functional Materials, ZJU-Hangzhou Global Scientific and Technological Innovation Center, Zhejiang University, Hangzhou 311215, P. R. China

^c Department of Chemistry, University of Pennsylvania, Philadelphia, Pennsylvania 19104, United States

† These authors contributed equally to this work.

Corresponding author: e-mail: zhijiechen@zju.edu.cn

Table of Contents

| | |
|--------------------------------------------------------------------|----|
| 1. Materials and general procedures | 2 |
| 2. Synthesis of ligands | 4 |
| 3. Synthesis of MOFs..... | 8 |
| 4. Single crystal X-ray data..... | 10 |
| 5. Additional figures | 13 |
| 6. Topological analysis | 16 |
| 7. PXRD patterns..... | 18 |
| 8. SEM images and energy dispersive X-ray spectroscopy (EDS) | 20 |
| 9. Low-pressure sorption measurements..... | 22 |
| 10. High-pressure sorption measurements..... | 27 |
| 11. References | 32 |

1. Materials and general procedures

Materials

[Fe₃O(CH₃COO)₆(H₂O)₃]Cl·6H₂O clusters were synthesized following a literature procedure.¹ 1,3,5-Tribromobenzene, (4-(methoxycarbonyl)phenyl)boronic acid, bis(pinacolato)diboron, sodium hydroxide, sodium carbonate (Na₂CO₃), potassium acetate (KOAc), potassium phosphate tribasic (K₃PO₄), magnesium sulfate (MgSO₄), 1,3,6,8-tetrabromopyrene were purchased from *Bidepharm*. Pd(PPh₃)₄, PdCl₂(dppf), Pd SPhos Gen III catalyst were purchased from *Energy chemical*. Acetone, THF, 1,4-dioxane, toluene, methanol (MeOH), ethanol (EtOH), dichloromethane (DCM), trichloromethane (CHCl₃), petroleum ether (PE), *N, N*-dimethylformamide (DMF) and acetic acid (HAc) were purchased from *Sinopharm*. All reagents were obtained from commercial sources and used without further purification, unless otherwise noted.

X-ray diffraction analyses.

Powder X-ray diffraction (PXRD) of MOFs was measured at room temperature on a Rigaku smartlab X-ray diffractometer powder diffractometer equipped with an asymmetric curved Germanium monochromator (CuK α 1 radiation, $\lambda = 1.54056 \text{ \AA}$) and one-dimensional silicon strip detector (MYTHEN2 1K from DECTRIS and D/teX Ultra 250). The line focused Cu X-ray tube was operated at 40 kV and 30 mA. The activated powder was sandwiched between two Kapton foils and measured in transmission geometry in a rotating holder. Data were measured over the range of 3-30°.

Gas sorption measurements.

Low-pressure nitrogen(N₂) isotherms measurements were carried at 77 K using JW-BK200C instrument. Methane isotherms measured on a micromeritics 3Flex at 278K, 288K, 298K and 308K.

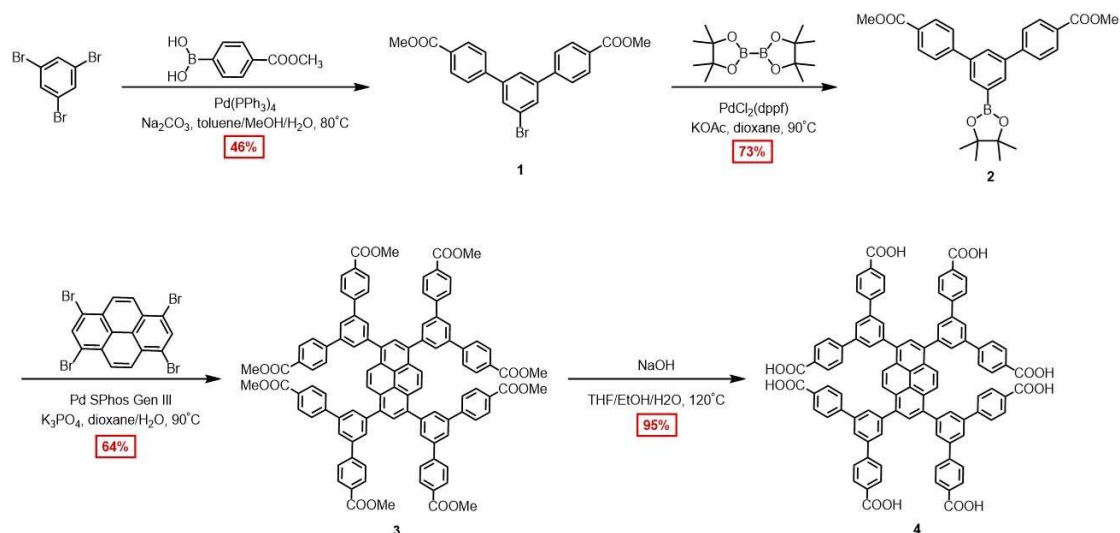
High-pressure methane isotherms measurements were performed at different temperatures using a high-pressure gas adsorption analyzer (BSD-PH).

Scanning electron micrographs (SEM)

SEM images were taken using a Scios2 Hivac (Thermo Fisher Scientific). Samples were deposited on conductive adhesive.

2. Synthesis of ligands

2.1 Synthetic protocols for H₈TBPP



Scheme S1. Synthesis of H₈TBPP

Dimethyl 5'-bromo-(1,1':3',1''-terphenyl)-4,4''-dicarboxylate (1): The compound **1** was synthesized according to the reported procedure with modifications.² 1,3,5-Tribromobenzene (10.0 g, 32 mmol), (4-(methoxycarbonyl)phenyl)boronic acid (15 g, 80 mmol), Na₂CO₃ (17 g, 160 mmol), [Pd(PPh₃)₄] (1.5 g, 1.27 mmol) were added to a three-necked flask that contained degassed toluene–MeOH–water (160:80:80 mL). The solution was stirred under N₂ atmosphere for 50 h under reflux. The product was extracted using DCM (160 mL×3), washed with brine (160 mL), and dried with anhydrous MgSO₄. The filtered solution was evaporated under reduced pressure. The residue was purified using column chromatography of silica gel (DCM/PE=1:4, V/V) to obtain compound **1**. Yield: 6.2 g (46 %).¹H NMR (400 MHz, CDCl₃) δ 8.14 (d, J = 8.5 Hz, 4H), 7.77 (d, J = 1.7 Hz, 2H), 7.75 (t, J = 1.7 Hz, 1H), 7.68 (d, J = 8.5 Hz, 4H), 3.96 (s, 6H) ppm.

Dimethyl 5'-pinacolatoborontel-(1,1':3',1''-terphenyl)-4,4''-dicarboxylate (2): Compound **1** (6.2 g, 14 mmol), bis(pinacolato)diboron (4.1 g, 15.4 mmol) and KOAc (11 g, 108mmol) were added to dioxane (300 mL) at room temperature under N₂ for 30 min, PdCl₂(dppf) (0.6 g, 0.8 mmol) was added. The reaction mixture was heated at 80 °C for 12 h under N₂. The mixture was extracted with CHCl₃ (120 mL×3), washed

with brine (120 mL). The combined organic extracts were dried over anhydrous MgSO_4 and the solvent removed under reduced pressure. The crude product was purified by flash chromatography using DCM/PE (3:1, V/V) as eluent to obtain a white solid. Yield: 5.0 g (73 %). ^1H NMR (400 MHz, CDCl_3) δ 8.12 (d, $J = 8.3$ Hz, 4H), 8.09 (s, 2H), 7.94 (s, 1H), 7.75 (d, $J = 8.4$ Hz, 4H), 3.95 (s, 6H), 1.39 (s, 12H) ppm.

MesTBPP (3). Compound **3** was synthesized by a Suzuki coupling reaction. Into a 250 mL flask were charged 1,3,6,8-tetrabromopyrene (0.51 g, 1 mmol), **2** (2.36 g, 5 mmol), Pd SPhos Gen III catalyst (117 mg, 0.15 mmol). The flask was degassed with N_2 , dioxane (80 mL) and aqueous K_3PO_4 solution (1 M, 20 mL) were added. The reaction was stirred at 90 °C for 2 days in N_2 atmosphere. The reaction solution was filtered and washed with water, and the resulting dark green filtrate was fully dissolved in CHCl_3 , CHCl_3 was removed under reduced pressure after filtered by diatomite. Then yellow-green products **3** were collected. Yield: 1.0 g (64 %). ^1H NMR (400 MHz, CDCl_3) δ 8.34 (s, 4H), 8.22 (s, 2H), 8.20-8.17 (d, $J = 9.0$ Hz, 4H), 8.15-8.11 (m, $J = 8.2, 4.5$ Hz, 16H), 7.96 (s, 8H), 7.80-7.77 (m, $J = 8.5$ Hz, 16H), 3.94 (s, 24H) ppm.

H₈TBPP (4). Compound **3** (0.5 g, 0.32 mmol) was suspended in 100 mL of a 1:1 mixture of EtOH and THF in a 250 mL round-bottom flask, followed by addition of 10 mL of 6 M NaOH (aq.). After the mixture was refluxed overnight, 4 M HCl (aq.) was slowly added until the pH was about 2. The precipitate was collected by filtration and washed with water, dried under vacuum to obtain green solid. Yield: 0.44 g (95 %). ^1H NMR (400 MHz, DMSO) δ 8.45 (s, 4H), 8.18 (s, 4H), 8.13-7.99 (m, 42H) ppm.

2.4. NMR spectroscopy

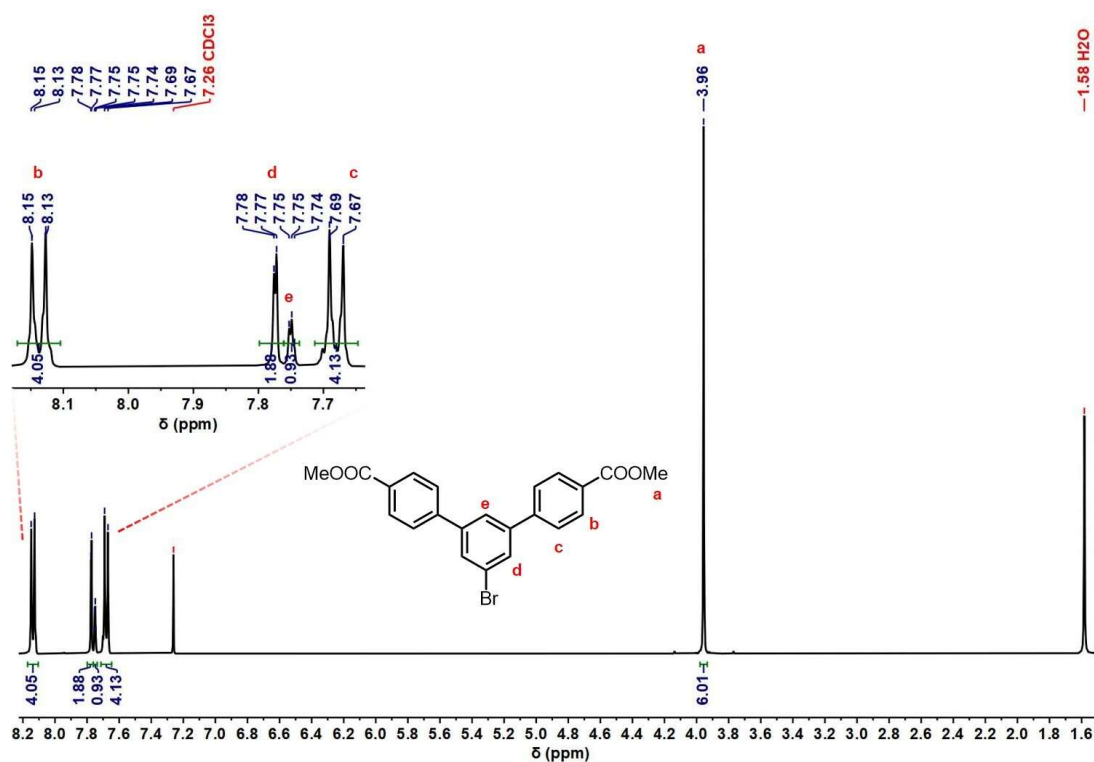


Figure S1. ¹H NMR spectrum (400 MHz, CDCl₃, 298 K) of compound 1.

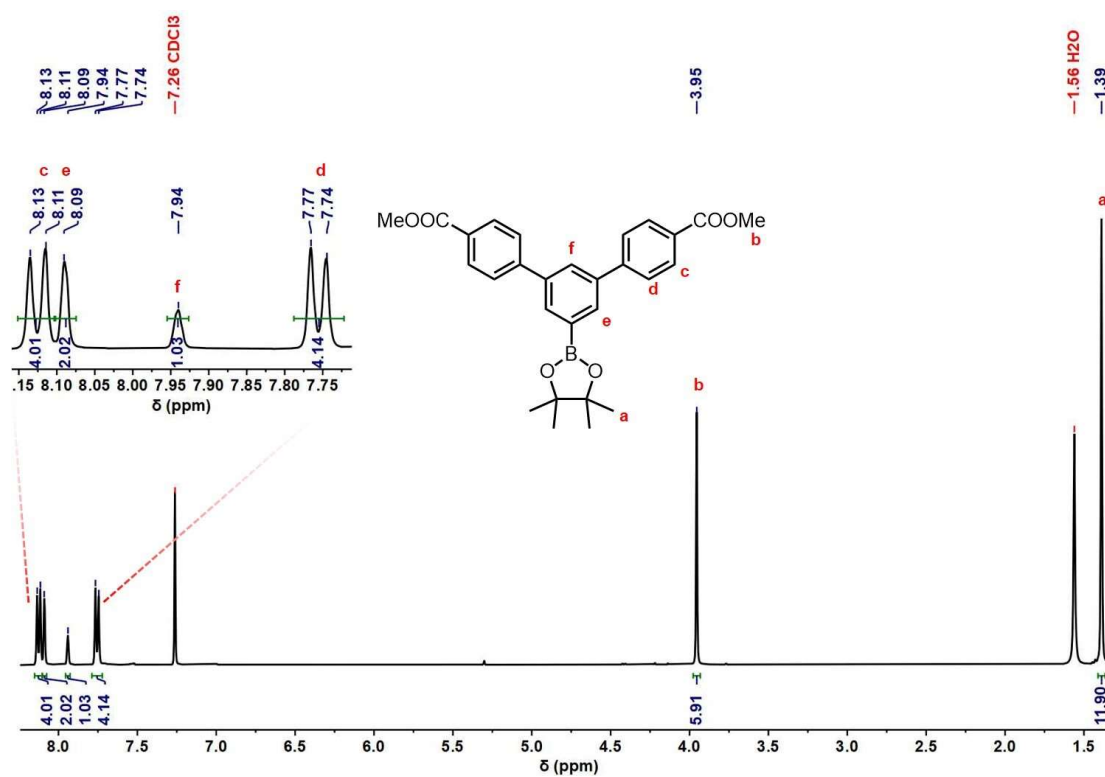


Figure S2. ¹H NMR spectrum (400 MHz, CDCl₃, 298 K) of compound 2.

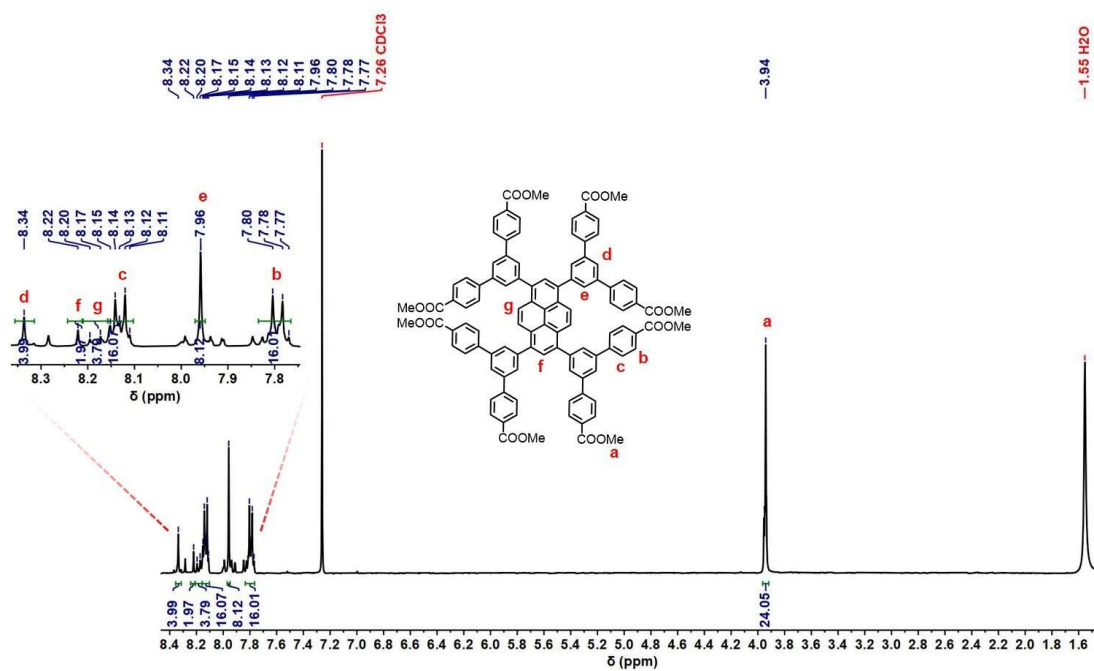


Figure S3. ^1H NMR spectrum (400 MHz, CDCl_3 , 298 K) of compound 3.

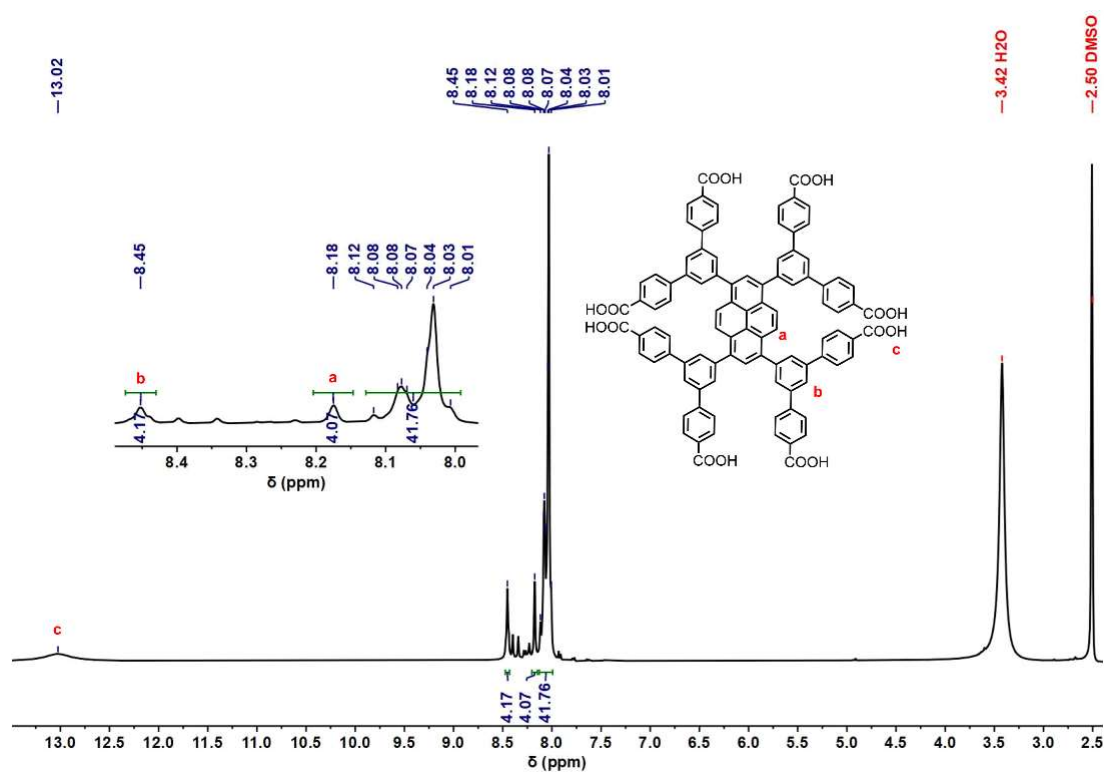


Figure S4. ^1H NMR spectrum (400 MHz, $\text{DMSO}-d_6$, 298 K) of compound 4.

3. Synthesis of MOFs

Synthesis of single crystal of Fe-TBPP-MOF

Fe₃O-cluster (10 mg) and H₈TBPP (5 mg) were dissolved in 2 mL of DMF, and 1 mL HAc in a 15 mL vial. Then, the mixture was sonicated for 3 min. The resultant mixture was sealed and heated to 150°C for 12 h. Golden block crystals were obtained (4.9 mg, 88%). Crystals were harvested and washed with DMF 6 times over three days. Then the crystals were washed with EtOH 6 times over three days. After washing by EtOH, the crystals were activated by supercritical CO₂ (sc-CO₂) followed by evacuating under vacuum at room temperature for 12 hours yielded activated MOFs.

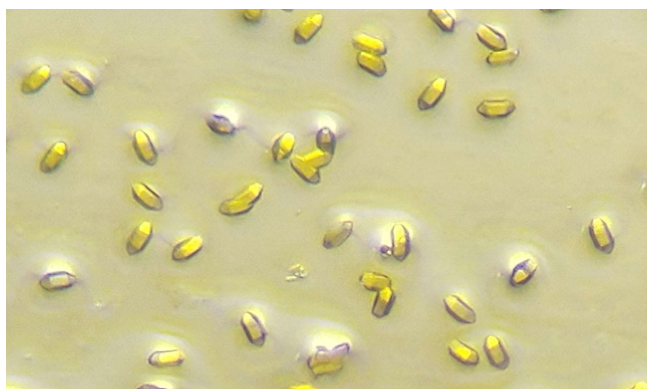


Figure S5. Optical images of the single crystals of Fe-TBPP-MOF.

Synthesis of single crystals of Cr-TBPP-MOF

The crystals of **Fe-TBPP-MOF** (about 50 mg) were transferred to a 15 mL Schlenk tube and aspirate as much DMF as possible, freeze pump the solution, charge with N₂, and repeat the cycle three times. In an argon atmosphere glovebox, 400 mg of CrCl₂ was dissolved in 6 mL of DMF and the CrCl₂/DMF solution was added to a Shrek bottle containing **Fe-TBPP-MOF** single crystals, and then sealed, taken out of the glovebox. The resultant mixture was put into a preheated oven at 120°C for 18 h. After the vial was cooled to room temperature, the green crystals were collected. These crystalline materials were washed 3 times with DMF and then soaked in DMF overnight. The crystals were washed with EtOH 6 times over three days. After soaking in DMF and EtOH, the crystals were activated by sc-CO₂ followed by evacuating under vacuum at 150°C for 12 hours yielded activated MOFs.

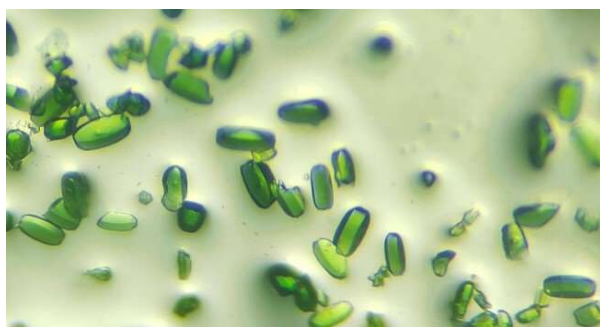


Figure S6. Optical images of the single crystals of **Cr-TBPP-MOF**.

4. Single crystal X-ray data

The single crystal X-ray diffraction (SCXRD) data of **Fe-TBPP-MOF** and **Cr-TBPP-MOF** were collected at 273 K and 275 K, respectively, using the BL17B Macromolecular Crystallography beamline of the State Key Laboratory of Protein Science at the Shanghai Synchrotron Radiation Facility (SSRF). The collected diffraction data were processed with the APEX 4 software program with included SAINT and SADABS programs. Intensities of reflections for the sample absorption were corrected using multi-scan method. Structures were solved by intrinsic phasing method and refined anisotropically with weighted full-matrix least squares on F^2 using SHELXT 6³ and SHELXL 7⁴ programs with Olex 2-1.5 graphic interface⁵.

All atoms except hydrogen atoms and water molecules were refined by full-matrix least-squares techniques with anisotropic displacement parameters, and the hydrogen atoms were geometrically fixed at the calculated positions attached to their parent atoms, treated as riding atoms. The benzene ring atoms were geometrically restrained to fit idealized six membered, respectively. DFIX, SIMU, ISOR and DANG restraints were used to obtain reasonable parameters. All crystal data and structure refinement parameters are summarized in **Table S1-S2**. CCDC 2385228-2385229 contain the supplementary crystallographic data for this paper. The data can be obtained free of charge from The Cambridge Crystallographic Data Centre via www.ccdc.cam.ac.uk/data_request/cif. Responses for the checkcif A-Alerts and B-Alerts for the two crystal structures were illustrated.

Table S1. Crystallographic data of Fe-TBPP-MOF.

| | Fe-TPBB-MOF |
|--------------------------------------------------------------|-------------------------------------------------------------------------------|
| Empirical formula | C ₁₉₂ H ₁₀₀ Fe ₆ O ₃₈ |
| Formula weight | 3349.81 |
| Temperature/K | 273.0 |
| Crystal system | monoclinic |
| Space group | <i>P</i> 2 ₁ |
| <i>a</i> /Å | 27.880(9) |
| <i>b</i> /Å | 19.220(7) |
| <i>c</i> /Å | 40.725(15) |
| α /° | 90 |
| β /° | 94.444(10) |
| γ /° | 90 |
| Volume/Å ³ | 21757(13) |
| <i>Z</i> | 2 |
| ρ_{calc} /cm ³ | 0.511 |
| μ /mm ⁻¹ | 0.225 |
| F(000) | 3424.0 |
| Crystal size/mm ³ | 0.05 × 0.02 × 0.01 |
| Radiation | synchrotron ($\lambda = 0.68883$) |
| 2 Θ range for data collection/° | 1.71 to 37.74 |
| Index ranges | -25 ≤ <i>h</i> ≤ 25, -17 ≤ <i>k</i> ≤ 17, -37 ≤ <i>l</i> ≤ 37 |
| Reflections collected | 47573 |
| Independent reflections | 30836 [<i>R</i> _{int} = 0.0584, <i>R</i> _{sigma} = 0.1072] |
| Data/restraints/parameters | 30836/1875/1754 |
| Goodness-of-fit on F ² | 0.957 |
| Final <i>R</i> indexes [<i>I</i> ≥ 2 σ (<i>I</i>)] | <i>R</i> ₁ = 0.0489, <i>wR</i> ₂ = 0.1142 |
| Final <i>R</i> indexes [all data] | <i>R</i> ₁ = 0.0704, <i>wR</i> ₂ = 0.1226 |
| Largest diff. peak/hole / e Å ⁻³ | 0.30/-0.42 |
| Flack parameter | 0.479(17) |

Table S2. Crystallographic data of **Cr-TBPP-MOF**.

| Cr-TBPP-MOF | |
|--------------------------------------------------------------|-------------------------------------------------------------------------------|
| Empirical formula | C ₁₉₂ H ₁₀₀ Cr ₆ O ₃₈ |
| Formula weight | 3326.71 |
| Temperature/K | 275.0 |
| Crystal system | monoclinic |
| Space group | <i>P</i> 2 ₁ |
| <i>a</i> /Å | 27.956(7) |
| <i>b</i> /Å | 18.611(5) |
| <i>c</i> /Å | 40.282(11) |
| α /° | 90 |
| β /° | 93.679(6) |
| γ /° | 90 |
| Volume/Å ³ | 20914(10) |
| <i>Z</i> | 2 |
| ρ_{calc} /cm ³ | 0.528 |
| μ /mm ⁻¹ | 0.182 |
| F(000) | 3400.0 |
| Crystal size/mm ³ | 0.1 × 0.05 × 0.02 |
| Radiation | synchrotron ($\lambda = 0.7085$) |
| 2 Θ range for data collection/° | 1.722 to 41.63 |
| Index ranges | -27 ≤ <i>h</i> ≤ 27, -18 ≤ <i>k</i> ≤ 18, -40 ≤ <i>l</i> ≤ 40 |
| Reflections collected | 151447 |
| Independent reflections | 41477 [<i>R</i> _{int} = 0.0976, <i>R</i> _{sigma} = 0.1097] |
| Data/restraints/parameters | 41477/2761/1694 |
| Goodness-of-fit on F ² | 1.042 |
| Final <i>R</i> indexes [<i>I</i> ≥ 2 σ (<i>I</i>)] | <i>R</i> ₁ = 0.0705, <i>wR</i> ₂ = 0.1890 |
| Final <i>R</i> indexes [all data] | <i>R</i> ₁ = 0.1020, <i>wR</i> ₂ = 0.2178 |
| Largest diff. peak/hole / e Å ⁻³ | 0.69/-0.47 |
| Flack parameter | 0.53(2) |

5. Additional figures

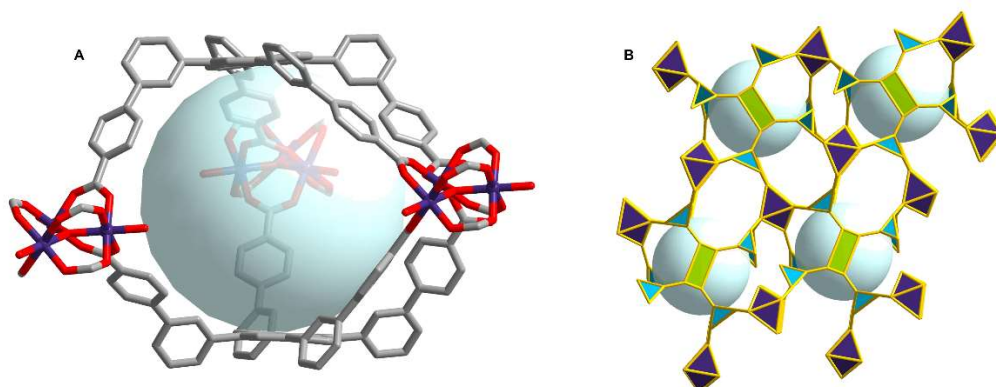


Figure S7. (A) The cavity of **M-TBPP-MOF**. (B) The related augmented net of cavity. Hydrogen atoms are omitted for clarity. Atoms of C, O, M are represented by grey, red, purple.

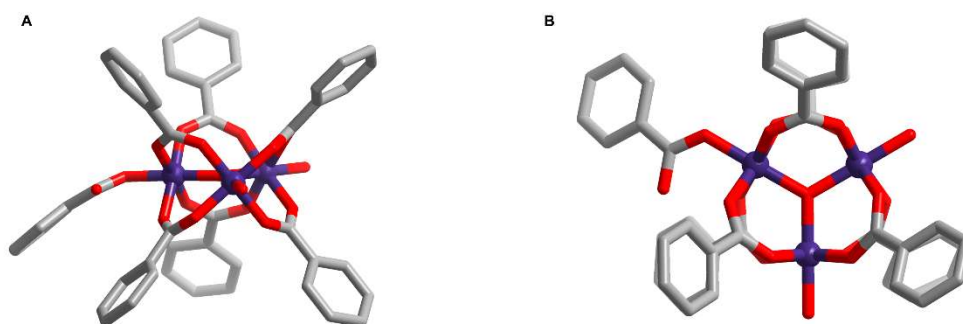


Figure S8. The coordination modes of trinuclear clusters. (A) Side view and (B) Top view. Hydrogen atoms are omitted for clarity. Atoms of C, O, M are represented by grey, red, purple.

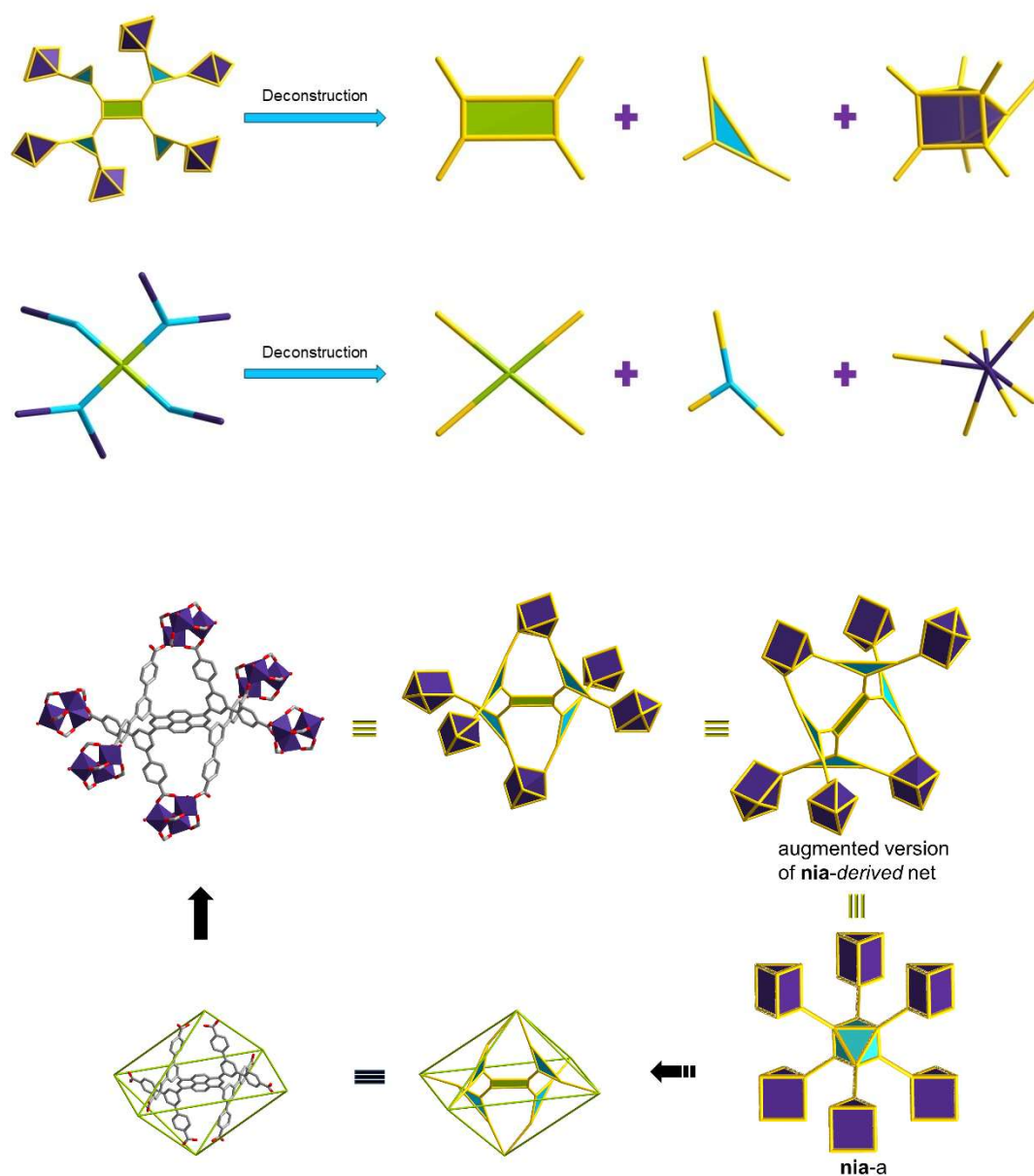


Figure S9. Simplified network connectivity showing the topology for **M-TBPP-MOF** (organic ligand node: green and blue; inorganic cluster node: purple). Hydrogen atoms are omitted for clarity.

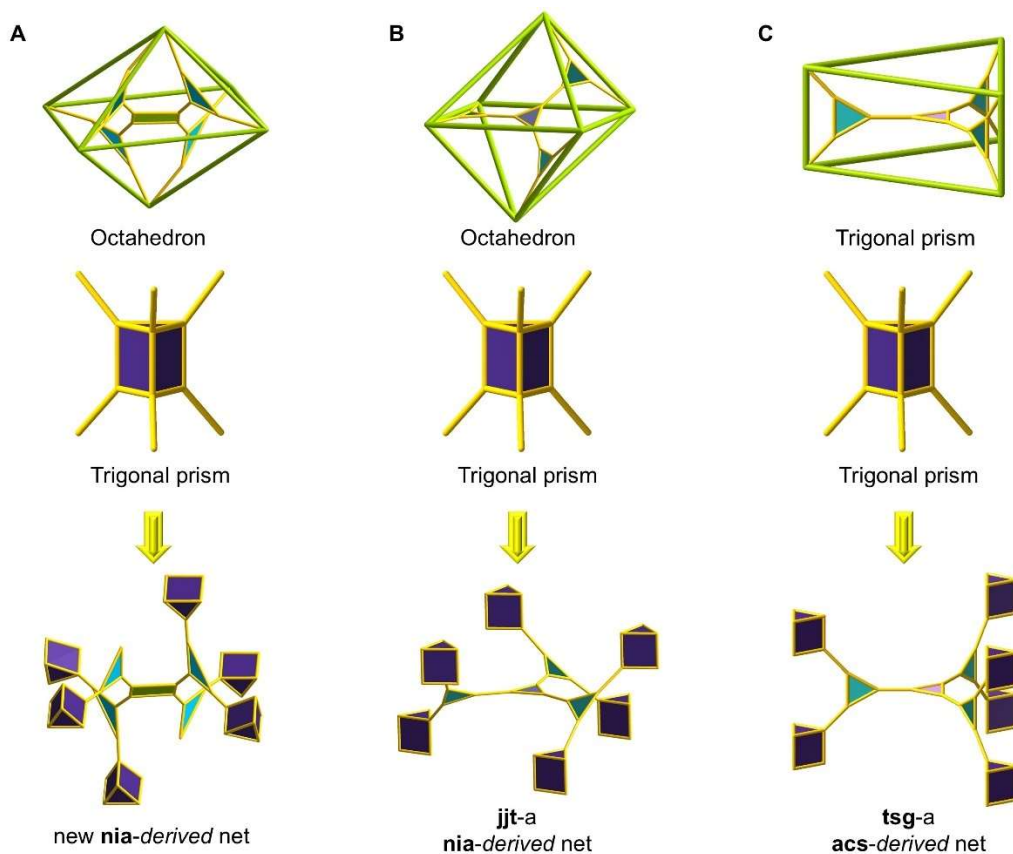


Figure S10. Comparison of selected *nia* and *acs* derived nets: (A) *nia*-derived net (the underlying net of **M-TBPP-MOF**), (B) *jjt* (*nia*-derived) net and (C) *tsg* (*acs*-derived) net.

6. Topological analysis

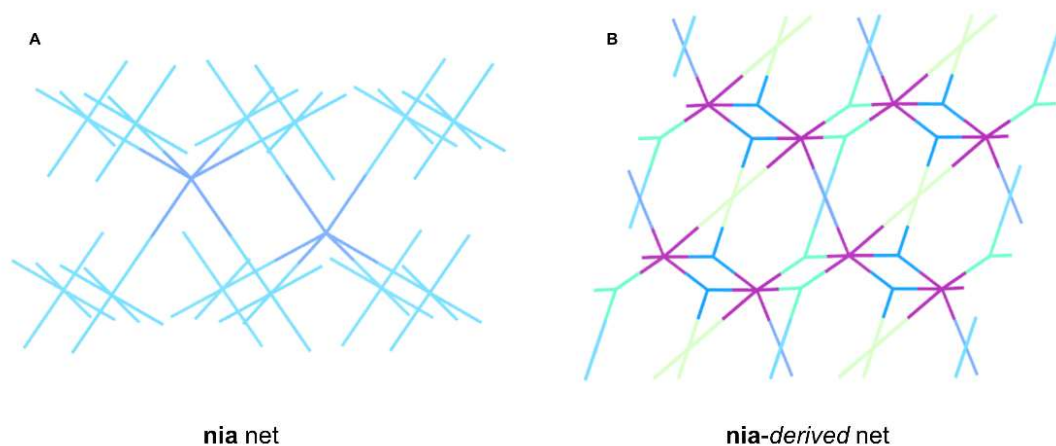


Figure S11. Topology schematic diagram of **nia** net and **nia-derived** net.

Vertex symbols for selected sublattice

 La1 Point symbol: $\{4^2.6^2.7.8\}$

Extended point symbol: $[4.4.6.6.7(2).8(6)]$

 Pr1 Point symbol: $\{5^2.6^2.8^2\}$

Extended point symbol: $[5.5.6.6.8(6).8(8)]$

 Eu1 Point symbol: $\{4.6^2\}$

Extended point symbol: $[4.6.6]$

 Ac1 Point symbol: $\{4^2.6\}$

Extended point symbol: $[4.4.6(2)]$

 Pa1 Point symbol: $\{5^2.6\}$

Extended point symbol: $[5.5.6]$

 Fm1 Point symbol: $\{4^2.5^2.6^4.7^6.8^5.9^2\}$

Extended point

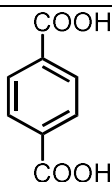
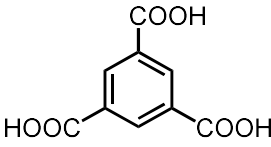
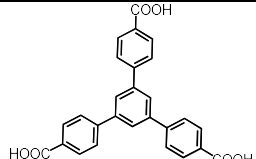
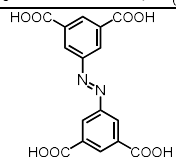
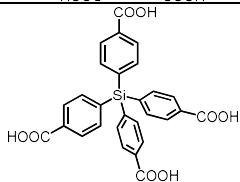
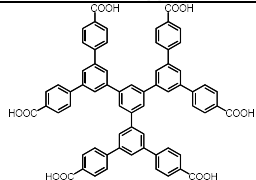
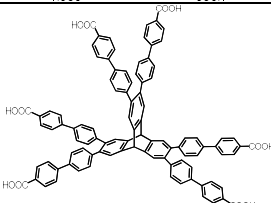
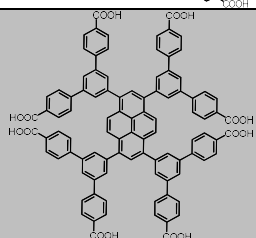
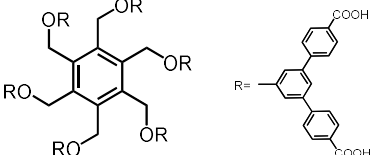
symbol: $[4.4.5.5.6.6.6.6.7.7.7.7(2).7(3).7(4).8.8(2).8(2).8(3).8(4).9.9(4)]$

 Point symbol for net:

$\{4.6^2\}^2 \{4^2.5^2.6^4.7^6.8^5.9^2\}^2 \{4^2.6^2.7.8\} \{4^2.6\}^2 \{5^2.6^2.8^2\} \{5^2.6\}^2$

$3^3,4^2,7$ -c net with stoichiometry $(3-c)2(3-c)2(3-c)2(4-c)(4-c)(7-c)2$; 6-nodal net

Table S3. Selected MOFs based on trimeric units and multicarboxylic acids.

| MOFs | Ligand connectivity | Ligand | Ref. |
|---------------------|---------------------|--------------------------------------------------------------------------------------|-----------|
| MIL-101 | 2 |  | 6 |
| MIL-100 | 3 |  | 7 |
| Sc-btb | |  | 8 |
| PCN-250 | 4 |  | 9 |
| PCN-264 | |  | 9 |
| Al-nia-mof-1 | 6 |  | 10 |
| NU-1501 | |  | 11 |
| M-TBPP-MOF | 8 |  | This work |
| In- alb -MOF | 12 |  | 12 |

7. PXRD patterns

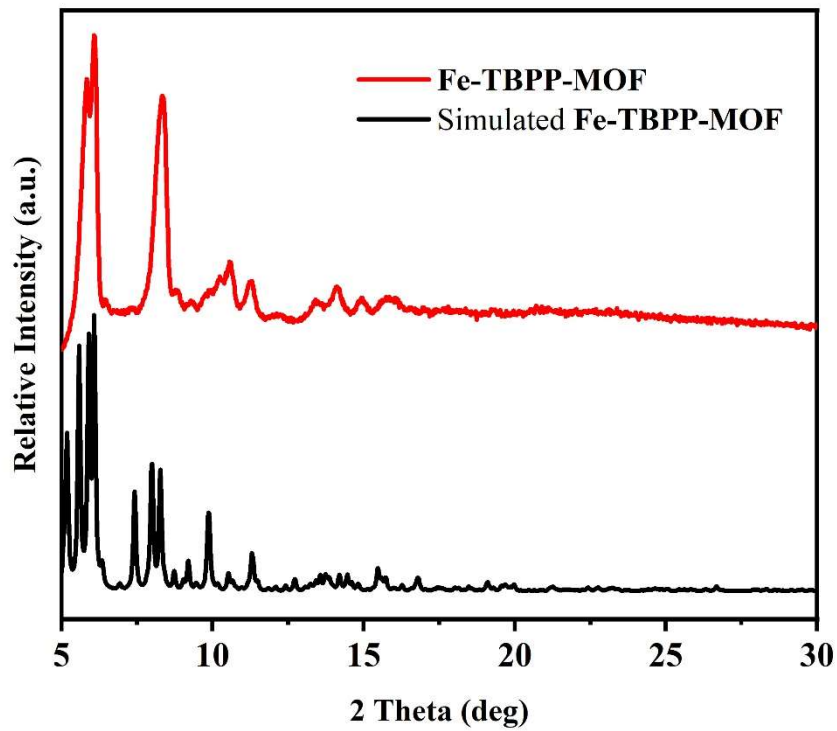


Figure S12. Experimental PXRD patterns of Fe-TBPP-MOF, in comparison to the simulated pattern from the crystal structure.

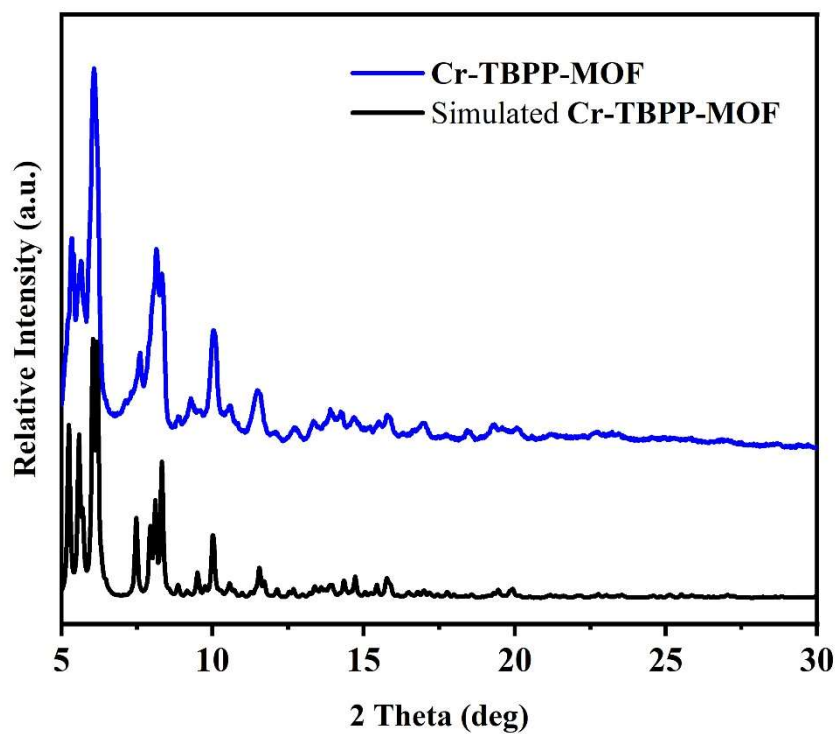


Figure S13. Experimental PXRD patterns of **Cr-TBPP-MOF**, in comparison to the simulated pattern from the crystal structure.

8.SEM images and energy dispersive X-ray spectroscopy (EDS)

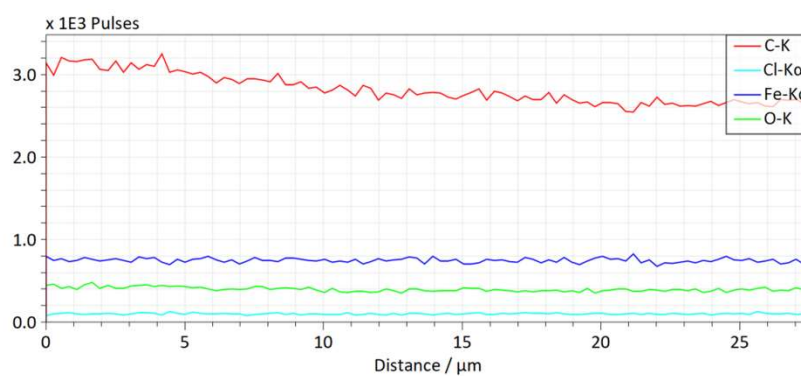
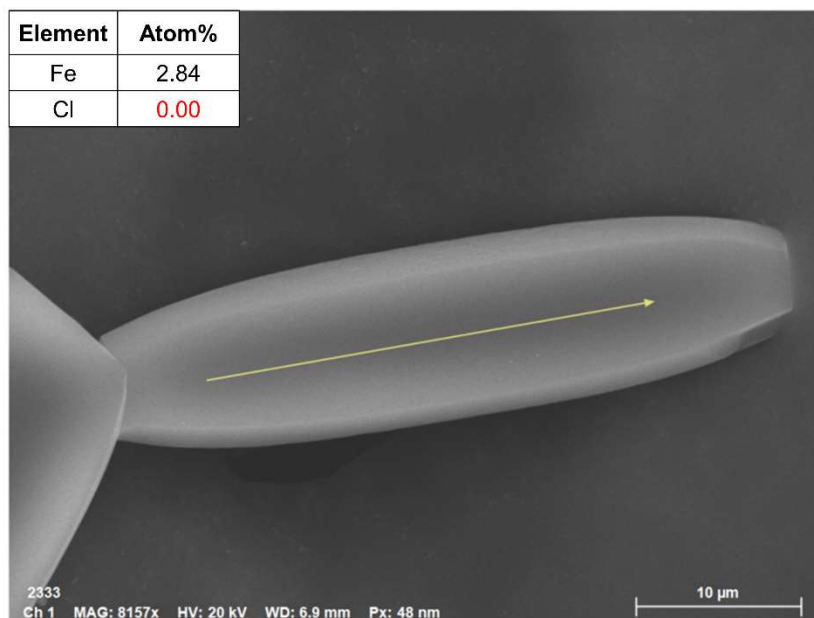


Figure S14. A SEM image with EDS elemental line scan analysis for **Fe-TBPP-MOF**.

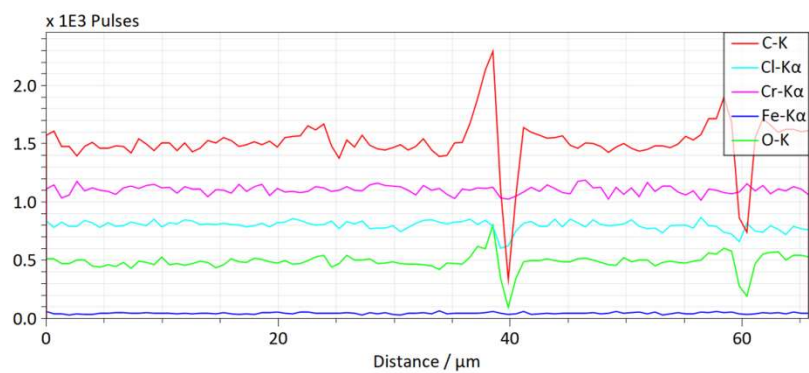
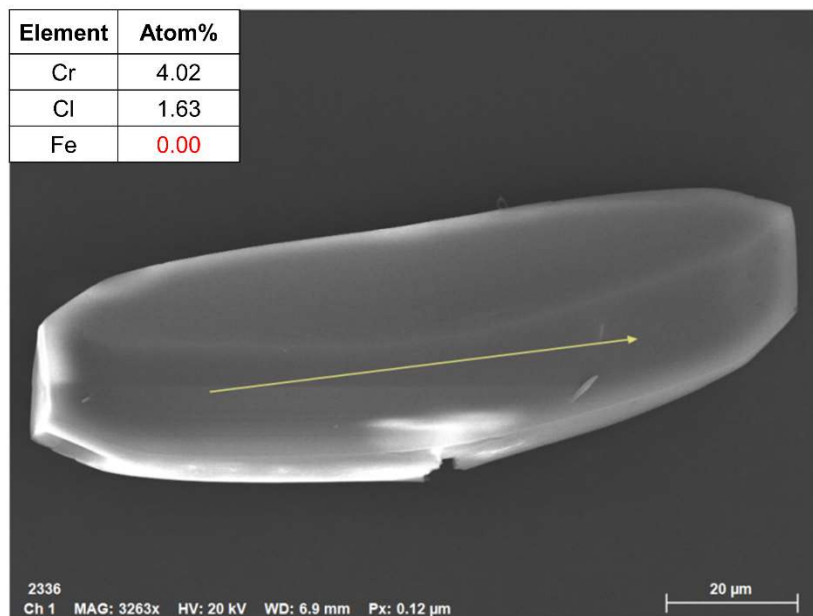


Figure S15. A SEM image with EDS elemental line scan analysis for **Cr-TBPP-MOF**.

9. Low-pressure sorption measurements

The sc-CO₂ drying was applied to activate **Fe-TBPP-MOF** and **Cr-TBPP-MOF**. Before doing the sc-CO₂ drying, the as synthesized materials were soaked in DMF for 3 days. The solvent was refreshed every 12 h, for each time, 12 mL of fresh DMF was added into the vials (or tubes). After three days, the DMF solvent was removed. The materials were then soaked in the EtOH for 3 days to fully exchange with the DMF in the materials. During this time, the EtOH was refreshed every 12 h and 10 mL of fresh EtOH was added into the vials (or tubes) each time. After removing solvents, the material was transferred to a small glass container for sc-CO₂ drying. After sc-CO₂ activation, **Fe-TBPP-MOF** was activated at room temperature and **Cr-TBPP-MOF** was activated at 150°C for 6 hours under a dynamic vacuum on BK200C.

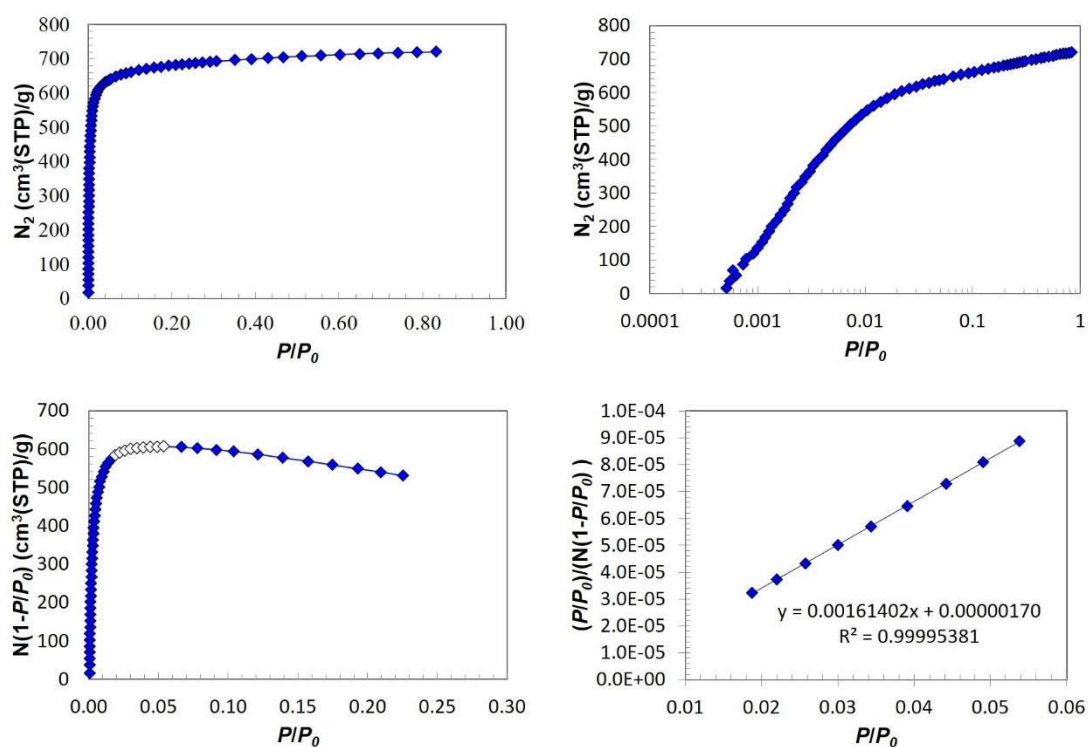


Figure S16. Experimental N₂ adsorption isotherm at 77 K of **Fe-TBPP-MOF**, and the region of selected points (white) used for the calculation of BET surface area, fulfilling all four BET criteria with R² higher than 0.995.

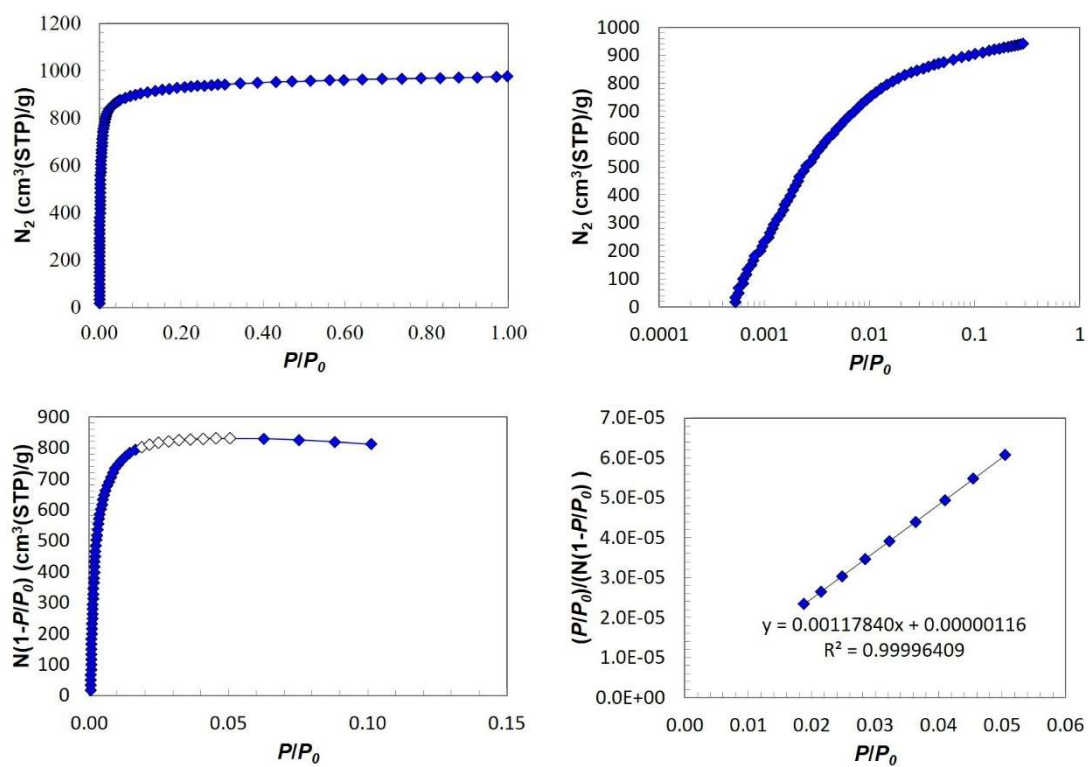


Figure S17. Experimental N₂ adsorption isotherm at 77 K of Cr-TBPP-MOF, and the region of selected points (white) used for the calculation of BET surface area, fulfilling all four BET criteria with R^2 higher than 0.995.

Table S4. Measured and simulated properties for TBPP-MOFs.

| Materials | Gravimetric BET area (m ² g ⁻¹) | Crystallographic density (g cm ⁻³) | Pore diameter (Å) | Pore volume (exp. ^a /sim. ^b) (cm ³ g ⁻¹) | Volumetric BET area ^c (m ² cm ⁻³) |
|---------------------|--------------------------------------------------------------|---------------------------------------------------|-------------------------|-------------------------------------------------------------------------------------------------|---------------------------------------------------------------------------|
| Cr- TBPP- MOF | 3700 | 0.53 | ~11.8 | 1.31/1.41 | 1961 |
| Fe-TBPP- MOF | 2700 | 0.51 | ~11.8 | 1.10/1.40 | 1377 |

^a calculated by single point method at $P/P_0=0.90$. ^b calculated based on crystal structures or optimized structure. ^c calculated based on crystallographic density.

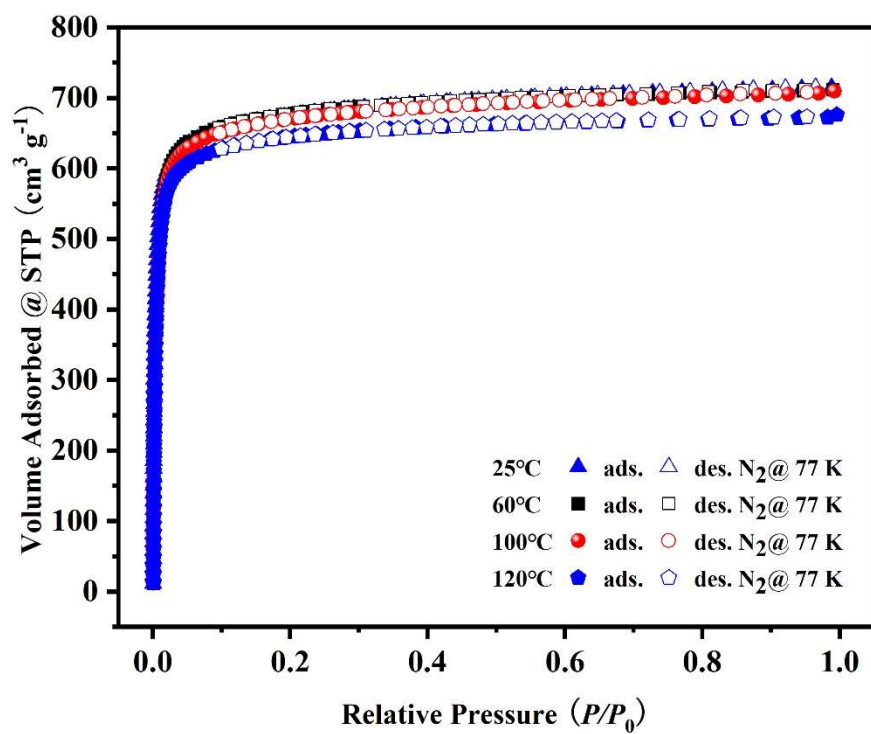


Figure S18. Experimental N₂ adsorption isotherms of Fe-TBPP-MOF at 77 K after different activation temperatures.

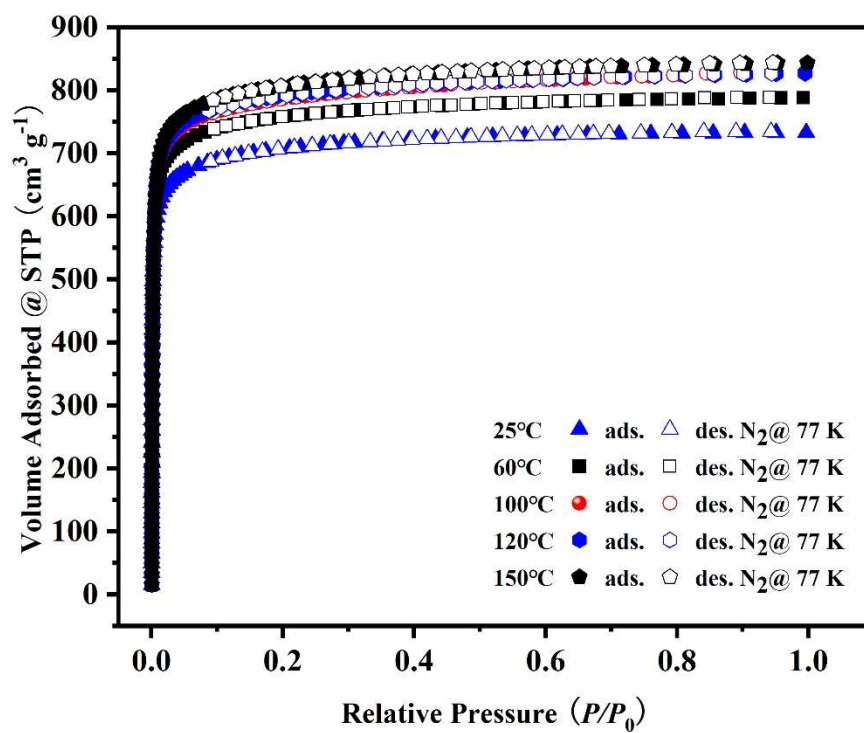


Figure S19. Experimental N₂ adsorption isotherms of Cr-TBPP-MOF at 77 K after different activation temperatures.

10. High-pressure sorption measurements

In our work, the volumetric storage capacity of MOFs was calculated with the ideal crystallographic density. Activated samples were packed under N₂ atmosphere before high pressure sorption measurements. Prior to the high-pressure sorption study, **Cr-TBPP-MOF** was activated under a dynamic vacuum for 12 h at 150 °C.

Comparison of adsorbed natural gas (ANG) and the coupling technology of liquefied natural gas (LNG) and ANG (LNG-ANG):

ANG is a method that utilizes porous materials to adsorb and store natural gas at ambient temperatures. The principle behind ANG is the physical adsorption of methane molecules into the pores of these porous materials. Compared to compressed natural gas (CNG), ANG can adsorb methane molecules at ambient temperature (~298 K) and relatively low pressure (e.g., 65 bar or 80 bar).

The LNG-ANG technology focuses on addressing practical issues encountered in commercial LNG transportation. Specifically, during the transportation or storage of LNG, the production of boil-off gas (BOG) is an inevitable phenomenon. Often, BOG is directly vented into the atmosphere, leading to both air pollution and energy waste. By integrating LNG with ANG storage, the cold energy and heat exchange derived from BOG enable the adsorbent to reach a cryogenic temperature (~159 K). Therefore, in the LNG-ANG mode, the adsorption process occurs at 159 K and 6 bar, while desorption takes place at 298 K and 5 bar. Compared to the traditional ANG method, these operating conditions substantially increase the working capacity of the adsorbent. Moreover, this low-temperature operation is achieved by recovering cold energy that would otherwise be wasted, making it economically viable.

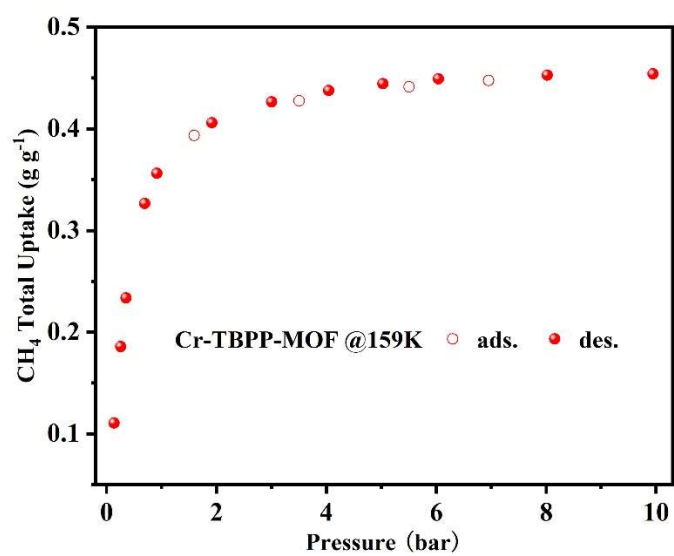
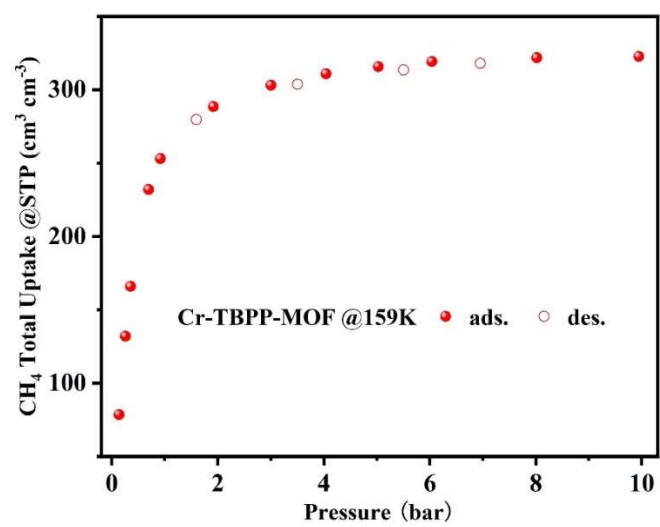


Figure S20. Methane sorption isotherms of Cr-TBPP-MOF recorded at 159 K.

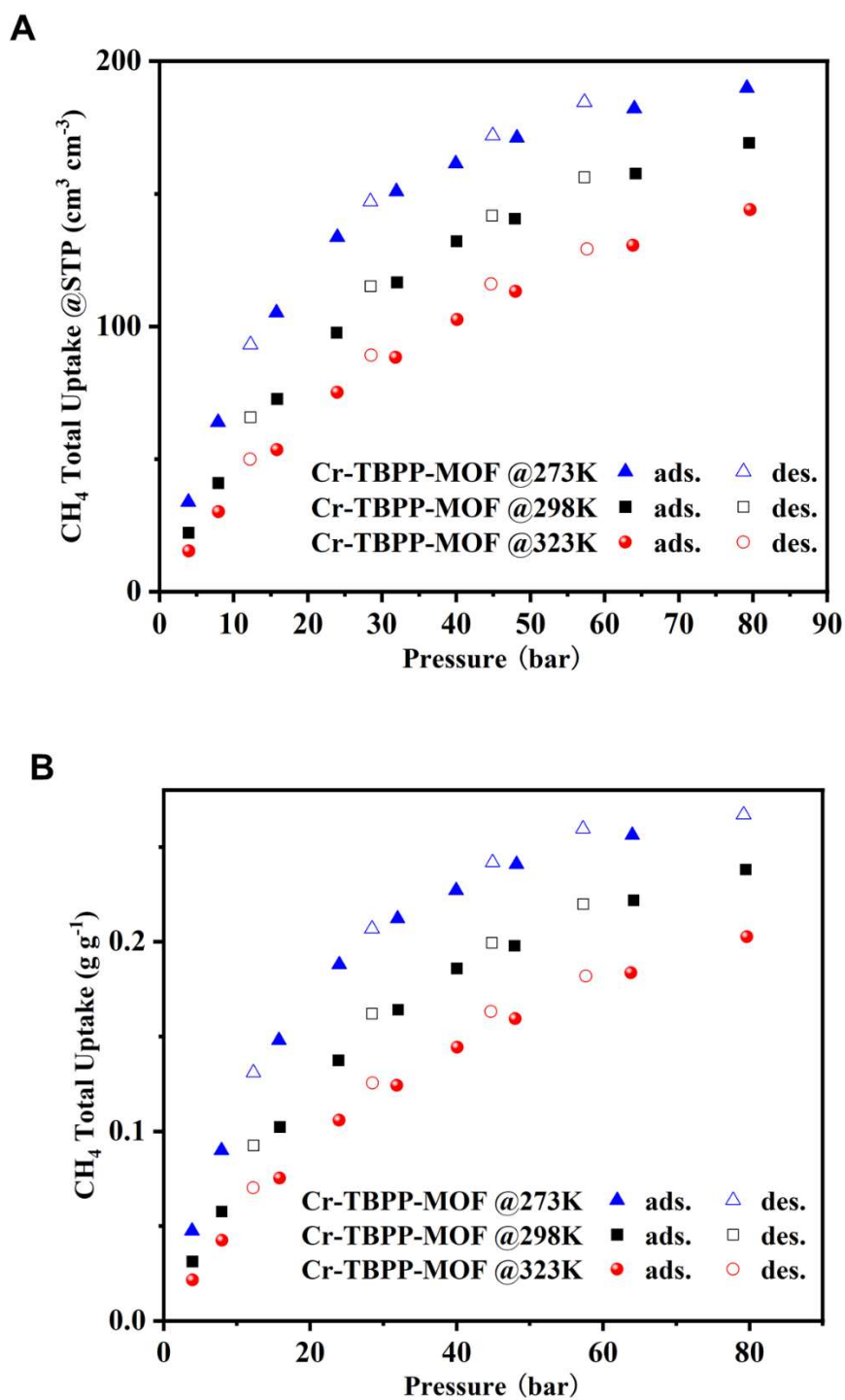


Figure S21. Volumetric (A) and gravimetric (B) sorption isotherms of methane for Cr-TBPP-MOF recorded at the indicated temperatures.

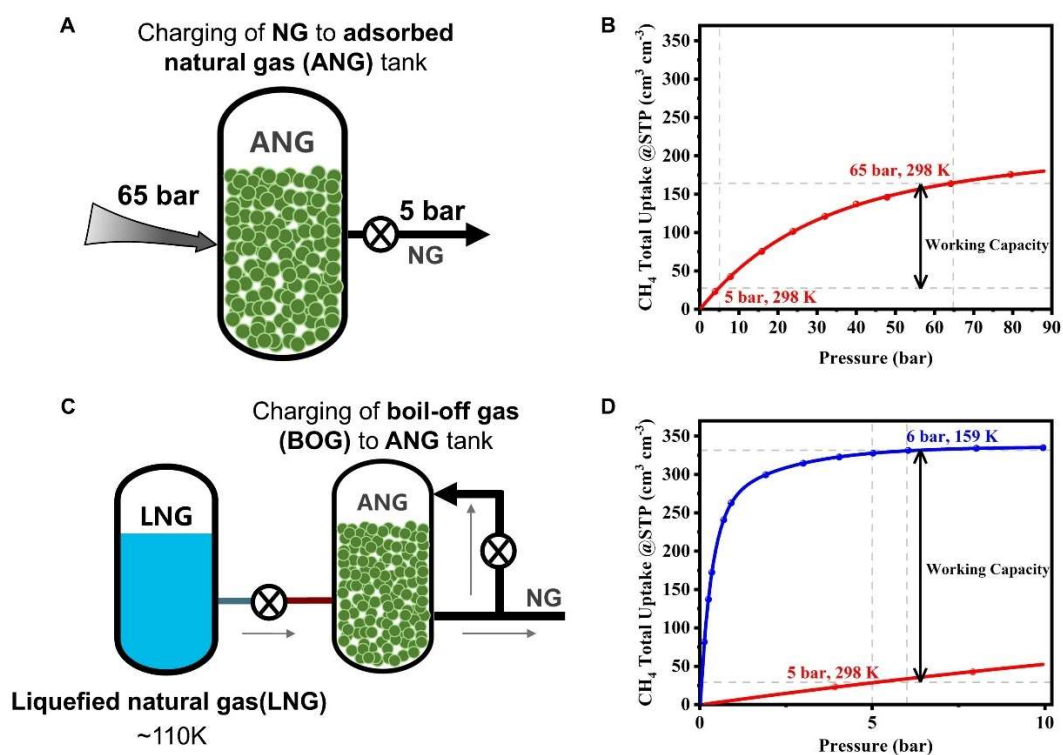


Figure S22. (A) Schematic of typical adsorbed natural gas (ANG) charging process. (B) Working capacity of **Cr-TBPP-MOF** under ANG-related conditions. (C) Schematic of ANG charging process coupled with liquefied natural gas (LNG) regasification process (i.e., LNG-ANG coupling). (D) Working capacity of **Cr-TBPP-MOF** under LNG-ANG-related conditions.¹³

Table S5. Comparison of some selected MOFs for methane storage capacity.

| | Density [g cm ⁻³] | PV [cm ³ g ⁻¹] | BET surface area [m ² g ⁻¹] | Storage capacity [cm ³ (STP) cm ⁻³] | | Working capacity [cm ³ (STP) cm ⁻³] | | Ref. |
|-----------------------------|----------------------------------|------------------------------------------|-------------------------------------------------------|---------------------------------------------------------------|---------------------------|---------------------------------------------------------------|--------------------------------------------|--------------|
| | | | | 298 K, 65 bar (ANG) | 159 K, 6 bar (LNG-ANG) | 298 K, 65 bar-5 bar (ANG) | 159 K, 6 bar- 298 K, 5 bar (LNG-ANG) | |
| HKUST-1 | 0.881 | 0.770 | 1850 | 267 | 324.1 | 190 | 249.1 | 14, 15 |
| MIL-53(Al) | 0.978 | 0.571 | 1223.4 | 186.8 | 311.8 | 137.3 | 262.3 | 15 |
| MIL-101(Cr) | 0.606 | 1.54 | 3302 | 215 | 275 | 180 | 240 | 15 |
| DUT-23(Co) | – | – | 5185 | 200.1 | 387.3 | 178.1 | 365.3 | 16 |
| DUT-23(Cu) | – | – | 5175 | 205.4 | 395.1 | 183.4 | 373.1 | 16 |
| uru-MOF-1 | 0.525 | 1.38 | 3170 | 143 | 330.2 | 122 | 309.4 | 17 |
| Cr-TBPP-MOF | 0.528 | 1.31 | 3700 | 164 | 331 | 137 | 302 | This work |
| PCN-14 | 0.829 | 0.85 | 2000 | 230 | – | 157 | – | 6 |
| MOF-210 | 0.25 | 3.60 | 6240 | 143 | – | 131 | – | 18 |
| Al-soc-MOF-1 | 0.34 | 2.09 | 5585 | 197 | – | 176 | – | 19 |
| MOF-519 | 0.953 | 0.94 | 2400 | 259 | – | 210 | – | 20 |
| MOF-905 | 0.549 | 1.34 | 3490 | 206 | – | 181 | – | 21 |
| AX-21 (activated carbon) | 0.487 | 1.64 | – | 203 | – | 155 | – | 22 |
| UTSA-20 | 0.909 | 0.66 | 1620 | 230 | – | 170 | – | 6 |
| NU-1501-Al | 0.283 | 2.91 | 7310 | 163(296K) | – | 147 | – | 11 |
| Ni-MOF-74 | 1.206 | 0.51 | 1350 | 259 | – | 129 | – | 6 |

11. References

1. D. Feng, K. Wang, Z. Wei, Y. P. Chen, C. M. Simon, R. K. Arvapally, R. L. Martin, M. Bosch, T. F. Liu, S. Fordham, D. Yuan, M. A. Omary, M. Haranczyk, B. Smit and H. C. Zhou, *Nat. Commun.*, 2014, **5**, 5723.
2. J. Jia, L. Wang, F. Sun, X. Jing, Z. Bian, L. Gao, R. Krishna and G. Zhu, *Chem. Eur. J.*, 2014, **20**, 9073-9080.
3. G. M. Sheldrick, *Acta Crystallogr A*, 2008, **64**, 112-122.
4. G. M. Sheldrick, *Acta Crystallogr C Struct Chem*, 2015, **71**, 3-8.
5. O. V. Dolomanov, L. J. Bourhis, R. J. Gildea, J. A. K. Howard and H. Puschmann, *J. Appl. Crystallogr.*, 2009, **42**, 339-341.
6. G. Férey, C. Mellot-Draznieks, C. Serre, F. Millange, J. Dutour, S. Surblé and I. Margiolaki, *Science*, 2005, **309**, 2040-2042.
7. G. Férey, C. Serre, C. Mellot-Draznieks, F. Millange, S. Surblé, J. Dutour and I. Margiolaki, *Angew. Chem. Int. Ed.*, 2004, **43**, 6296-6301.
8. I. A. Ibarra, X. Lin, S. Yang, A. J. Blake, G. S. Walker, S. A. Barnett, D. R. Allan, N. R. Champness, P. Hubberstey and M. Schröder, *Chem. Eur. J.*, 2010, **16**, 13671-13679.
9. D. Feng, K. Wang, Z. Wei, Y.-P. Chen, C. M. Simon, R. K. Arvapally, R. L. Martin, M. Bosch, T.-F. Liu, S. Fordham, D. Yuan, M. A. Omary, M. Haranczyk, B. Smit and H.-C. Zhou, *Nat. Commun.*, 2014, **5**, 5723.
10. D. Alezi, J. Jia, P. M. Bhatt, A. Shkurenko, V. Solovyeva, Z. Chen, Y. Belmabkhout and M. Eddaoudi, *Inorg. Chem.*, 2022, **61**, 10661-10666.
11. Z. Chen, P. Li, R. Anderson, X. Wang, X. Zhang, L. Robison, L. R. Redfern, S. Moribe, T. Islamoglu, D. A. Gomez-Gualdrón, T. Yildirim, J. F. Stoddart and O. K. Farha, *Science*, 2020, **368**, 297-303.
12. Z. Chen, Ł. J. Weseliński, K. Adil, Y. Belmabkhout, A. Shkurenko, H. Jiang, P. M. Bhatt, V. Guillerme, E. Dauzon, D.-X. Xue, M. O'Keeffe and M. Eddaoudi, *J. Am. Chem. Soc.*, 2017, **139**, 3265-3274.
13. Y. Zhong, Z. Xiong, Y. Li, H. Shi, R. Chen, H. Liang, Z. Qiao and Z. Chen, *Chem. Eng. J.*, 2024, DOI: 10.1016/j.cej.2024.157536.
14. Y. Peng, V. Krungleviciute, I. Eryazici, J. T. Hupp, O. K. Farha and T. Yildirim, *J. Am. Chem. Soc.*, 2013, **135**, 11887-11894.
15. S. Y. Kim, J. H. Kang, S. I. Kim and Y. S. Bae, *Chem. Eng. J.*, 2019, **365**, 242-248.
16. S. Y. Kim, S. Han, S. Lee, J. H. Kang, S. Yoon, W. Park, M. W. Shin, J. Kim, Y. G. Chung and Y. S. Bae, *Adv. Sci.*, 2022, **9**, e2201559.
17. L. Shi, Y. Zhong, H. Cao, H. Wang, Z. Xiong, K. Wang, H. Shen and Z. Chen, *Nat. Synth.*, 2024, DOI: 10.1038/s44160-024-00622-5.
18. H. Furukawa, N. Ko, Y. B. Go, N. Aratani, S. B. Choi, E. Choi, A. Yazaydin, R. Q. Snurr, M. O'Keeffe, J. Kim and O. M. Yaghi, *Science*, 2010, **329**, 424-428.

19. D. Alezi, Y. Belmabkhout, M. Suyetin, P. M. Bhatt, J. Weseliński Ł, V. Solovyeva, K. Adil, I. Spanopoulos, P. N. Trikalitis, A. H. Emwas and M. Eddaoudi, *J. Am. Chem. Soc.*, 2015, **137**, 13308-13318.
20. F. Gándara, H. Furukawa, S. Lee and O. M. Yaghi, *J. Am. Chem. Soc.*, 2014, **136**, 5271-5274.
21. J. C. Jiang, H. Furukawa, Y. B. Zhang and O. M. Yaghi, *J. Am. Chem. Soc.*, 2016, **138**, 10244-10251.
22. J. A. Mason, M. Veenstra and J. R. Long, *Chem. Sci.*, 2014, **5**, 32-51.